Spectral Interferometric Implementation with Passive Polarization Optics of Coherent Anti-Stokes Raman Scattering

Brad Littleton,[1,*] Thomas Kavanagh,[1] Frederic Festy,[2] and David Richards[1,†]

[1]*Department of Physics, King's College London, Strand, London, WC2R 2LS, United Kingdom*

[2]*Dental Institute, King's College London, Guy's Hospital, London Bridge, London SE1 9RT, United Kingdom*

(Received 13 March 2013; published 5 September 2013)

We have developed an interferometric implementation of coherent anti-Stokes Raman scattering which enables broadband coherent Raman spectroscopy free from the nonresonant background, with a signal strength proportional to concentration. Spectra encode mode symmetry information into the amplitude response, which can be directly compared to polarized spontaneous Raman spectra. The method requires only passive polarization optics and is suitable for a wide range of laser linewidths and pulse durations. The method's application to Raman spectral imaging is demonstrated.

DOI: 10.1103/PhysRevLett.111.103902 PACS numbers: 42.65.Dr, 33.20.Fb, 78.47.jh, 87.64.mn

Raman scattering provides a powerful optical route to obtain chemically specific information and is widely used in biology, chemistry, and materials science. Coherent Raman scattering (CRS) is the nonlinear multiphoton equivalent of the spontaneous Raman process and allows much faster acquisition [1,2], with additional benefits of intrinsic optical sectioning in microscopy [3] and rejection of sample luminescence [4]. In microscopic imaging, CRS has been very successfully employed for imaging individual Raman bands, but quantitative hyperspectral coherent Raman imaging of biological samples, analogous to spontaneous Raman microspectroscopy, has proven difficult to achieve, primarily due to the coherent backgrounds inherent to CRS [2]. Similarly, for gas-phase combustion studies, coherent backgrounds obscure weak resonances, distort line shapes, and complicate numerical analyses [5,6]. Dealing with these backgrounds increases acquisition times, complicating the application of CRS to time-varying reacting flows. In this Letter, we report on a new method for quantitative broadband CRS spectral imaging and demonstrate the method via microscopic imaging. The technique has relaxed requirements on spectral phase and instrument stability and provides full access to the Raman fingerprint region while retaining the advantages of enhanced signal and optical sectioning inherent to CRS.

The two most widely used CRS techniques are stimulated Raman scattering (SRS) and coherent anti-Stokes Raman scattering (CARS) [Fig. 1(a)] [4]. At intensities suitable for biological samples, SRS requires heterodyne methods [7,8] to detect the signal against the coherent background of the excitation fields; such methods require wavelength scanning to build up spectral information. CARS is a four wave mixing (FWM) process with a signal field generated at the anti-Stokes frequency $\omega_{aS} = \omega_{pr} + \omega_p - \omega_S$, which is spectrally separated from the excitation fields (ω_p, ω_S, and ω_{pr} are denoted as the pump, Stokes, and probe fields, respectively). CARS can therefore simultaneously generate an entire vibrational spectrum by using a spectrally broad Stokes beam [9], making it suitable for rapid detection of vibrational (and rotational) spectra.

The coherent background in CARS arises from FWM processes that are independent of vibrational transitions [Fig. 1(a)]. The anti-Stokes intensity is determined by the third order susceptibility

$$|\chi|^2 = \chi_{\mathrm{NR}}^2 + 2\chi_{\mathrm{NR}}\mathrm{Re}\{\chi_{\mathrm{R}}\} + |\chi_{\mathrm{R}}|^2, \qquad (1)$$

where χ_{R} and χ_{NR} are components resonant and nonresonant with vibrational modes, respectively. Since χ_{R} is

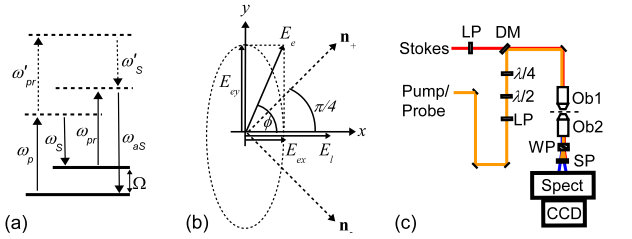

FIG. 1 (color online). (a) Energy level diagram. CARS involves the path $\omega_p \rightarrow \omega_S \rightarrow \omega_{pr} \rightarrow \omega_{aS}$; SRS is $\omega_p \rightarrow \omega_S \rightarrow \Omega$ (where Ω is a vibrational resonance). An example nonresonant FWM pathway is shown as $\omega_p \rightarrow \omega'_{pr} \rightarrow \omega'_S \rightarrow \omega_{aS}$. (b) Polarizations for SIP CARS with one elliptical (or circular) polarized field E_e and one linear field E_l. Detection is performed along $\mathbf{n}_+$ and $\mathbf{n}_-$. E_e is shown as the input to a $\lambda/4$ plate (orientated at an angle ϕ to the fast axis) to generate the desired elliptical polarization. For a circular Stokes and linear pump, $E_e = E_S$, $E_l = E_p = E_{pr}$, and $\phi = \pi/4$. For an elliptical pump and linear Stokes, $E_e = E_p = E_{pr}$, $E_l = E_S$, and $\phi = \pi/8$ or $3\pi/8$. (c) Experimental setup. Pump-probe ellipticity was controlled by a combination of linear polarizer (LP) and zero-order half- and quarter-wave plates ($\lambda/2$, $\lambda/4$). Beams were combined on a dichroic mirror (DM) and focused into the sample by a 1.3 NA objective lens (Ob1). An identical lens (Ob2) collected the signal, which was separated from the excitation fields by a short pass filter (SP) and dispersed via a spectrometer onto a CCD. A Wollaston prism (WP) separated the two detection polarizations on the CCD.

proportional to the number of resonant modes in a medium, the concentration dependence of CARS is quadratic and nonlinearly mixed with the nonresonant background (NRB). The interferometric (second) term, however, is linear in χ_R and is amplified by χ_{NR}. Re$\{\chi_R\}$ is dispersive and antisymmetric about the vibrational line center; however, Im$\{\chi_R\}$ is directly related to the spontaneous Raman spectrum [4].

Many methods have been developed to remove the NRB from CARS spectra [6,10]. Noninterferometric techniques, such as polarization-based [11–14] and time-resolved methods [15–17], recover a (typically small) proportion of the energy in the third term of Eq. (1). However, the interferometric term is the largest source of signal for weak resonances and, below the damage threshold of biological samples, CRS has been shown to be faster than spontaneous Raman spectroscopy only if this term is detected [2,18].

Im$\{\chi_R\}$ may be recovered through interference between the anti-Stokes field and a local oscillator (LO), which may be generated either externally [19–22] or by using the NRB as an internal LO [23–25]. Previous experimental implementations have stringent requirements on stability and coherence of the broadband laser source [24–30] or require phase scanning [23,30].

Computational internal LO approaches have been developed, which use the χ_{NR} Re$\{\chi_R\}$ term present in raw CARS spectra to calculate Im$\{\chi_R\}$ [31,32]. These techniques produce good approximations to Im$\{\chi_R\}$ if the spectra are of sufficient width but also intrinsically produce a spectrally varying error signal, which increases at resonances (up to 10%) [33]. They also require prior or postestimation of the spectral variation of the NRB (effectively the variation of the Stokes field) from a reference material, which is often compromised by the presence of a residual resonant response. Changes of the background spectrum during an acquisition lead to errors that can mask the weaker resonances in the fingerprint region of biological samples [2].

We describe here a new internal LO technique, spectral interferometric polarized CARS (SIP CARS), that is significantly simpler to implement than previous experimental approaches. It does not have stringent requirements on the lasers used and is suitable for narrow-band, multiline, and broadband systems. Transform limited pulses are not required, and supercontinua generated via photonic crystal fibers (PCF) can therefore be used to generate broad, NRB-free vibrational spectra. Furthermore, the NRB is removed without requiring an independent measurement of its spectral variation. The technique is similar to dual quadrature spectral interferometry [24,26,30,34], except that the fields have different frequencies and hence only interfere via the nonlinear response. The third-order response is solved exactly, without assumptions on the relative strength of resonant and nonresonant components [24,35].

To illustrate the method, consider CARS with a (right-hand) circularly polarized Stokes field and pump and probe fields linearly polarized along the x axis, as in Fig. 1(b). For convenience, we express the Stokes electric field in terms of the linear polarization E_S used to generate it via a $\lambda/4$ plate; so, the field along the x and y axes is $E_{S_x} = E_S/\sqrt{2}$ and $E_{S_y} = iE_S/\sqrt{2}$. The susceptibility can be separated into diagonal (e.g., χ_{iiii}) and off-diagonal (e.g., χ_{ijij}) elements; the off-diagonal terms mediate the coupling of orthogonally polarized excitations into the detected polarization. Considering the polarization P_+, induced in the medium along the $\hat{\mathbf{n}}_+$ axis, at $+\pi/4$ to the pump and probe polarization, we have

$$P_+ = \tfrac{1}{2}\chi_{1111}E_{pr}E_p(E_S^+)^* + \tfrac{1}{2}\chi_{1221}E_{pr}E_p(E_S^+)^* + \tfrac{1}{2}\chi_{1122}E_{pr}E_p(E_S^-)^* + \tfrac{1}{2}\chi_{1212}E_{pr}E_p(E_S^-)^*,$$

where E_p and E_{pr} are the electric fields of the pump and probe beams, and E_S^+ and E_S^- are the components of the Stokes field along $\hat{\mathbf{n}}_+$ and $\hat{\mathbf{n}}_-$, respectively [Fig. 1(b)]. As $E_S^+ = iE_S^-$, the last two terms lag the first two in phase by $\pi/2$. Imaginary components of the last two terms therefore interfere with real components of the first two, with the strength of the interference determined by the relative strength of the diagonal and off-diagonal tensor elements. Similarly, for P_-, the E_S^+ and E_S^- terms are swapped, and the last two terms lead the first two by $\pi/2$. Imaginary components are therefore added to the real components along $\hat{\mathbf{n}}_+$ and subtracted from them along $\hat{\mathbf{n}}_-$; spectral interferometric detection is performed by taking the difference between spectra measured at these polarizations, leaving the purely imaginary components [24].

The induced polarizations are more succinctly expressed within a basis including the pump and probe polarizations,

$$P_x = \frac{1}{\sqrt{2}}\chi_{1111}E_{pr}E_pE_S^*, \quad P_y = -\frac{i}{\sqrt{2}}\chi_{2112}E_{pr}E_pE_S^*. \quad (2)$$

Along the detection axes $\hat{\mathbf{n}}_+$ and $\hat{\mathbf{n}}_-$, the induced polarizations are $P_+ = (P_x + P_y)/\sqrt{2}$ and $P_- = (P_x - P_y)/\sqrt{2}$, and the anti-Stokes signals are $S_+ \propto P_+P_+^*$ and $S_- \propto P_-P_-^*$. The sum and difference of the anti-Stokes intensities are then $\Sigma S = S_+ + S_- \propto P_xP_x^* + P_yP_y^*$ and $\Delta S = S_+ - S_- \propto P_xP_y^* + (P_xP_y^*)^*$, respectively. The difference signal is therefore given by

$$\triangle S \propto \mathrm{Im}\{\chi_{1111}\chi_{2112}^*\}I_{pr}I_pI_S, \quad (3)$$

where $I_i = E_iE_i^*$ are the beam intensities. Separating the susceptibilities into resonant and nonresonant components $\chi_{ijkl} = \chi_{ijkl}^{NR} + \chi_{ijkl}^{R}$, assuming an isotropic medium ($\chi_{2112} = \chi_{1221}$, $\chi_{1111} = \chi_{1212} + \chi_{1221} + \chi_{1122}$), and noting that the nonresonant terms possess Kleinman symmetry [36] ($\chi_{1111}^{NR} = \chi_{NR}$, $\chi_{1212}^{NR} = \chi_{1122}^{NR} = \chi_{1221}^{NR} = \chi_{NR}/3$), this becomes

$$\begin{aligned}\triangle S &\propto \chi_{NR}\mathrm{Im}\{\chi_{1111}^R - 3\chi_{1221}^R\}I_{pr}I_pI_S \\ &\propto (1-3\rho)\chi_{NR}\mathrm{Im}\{\chi_{1111}^R\}I_{pr}I_pI_S, \end{aligned} \quad (4)$$

where $\rho = \chi^{R}_{1221}/\chi^{R}_{1111}$ is the CARS depolarization ratio of the resonance [37]. The difference spectrum is therefore linear in the imaginary component of χ, is amplified by χ_{NR}, and contains no real, dispersive terms or nonresonant contributions. Because of the linear response, well established linear multivariate analyses such as principal component analysis or cluster analysis can be applied. Mode symmetry information is mixed into the amplitude response through the depolarization ratio ρ ($0 < \rho < 3/4$).

Because the interference is effectively between $\pi/2$ phase shifted copies of the same fields, there are no extra requirements on the coherence of the excitation pulses. Moreover, if spectra are measured simultaneously, incoherent backgrounds (such as two-photon fluorescence) and any variation of the real components of the CARS signal are common mode in S_+ and S_- and are automatically subtracted out. This is essentially a balanced homodyne detection scheme, except that in this case, the signal arises in the low noise difference channel rather than the sum channel.

At the focus of a high NA lens, it is easier to control the circular polarization of a narrow-band beam rather than a broadband one, and, commonly, the pump and probe fields are supplied by the same beam, so $E_{pr} = E_p$. To address this, we can generalize Eq. (4) to the case of arbitrary ellipticity of both Stokes and pump beams (see the Supplemental Material [38]),

$$\triangle S \propto C(\theta, \phi) I_p^2 I_S (1 - 3\rho) \chi_{NR} \mathrm{Im}\{\chi^{R}_{1111}\}, \qquad (5)$$

where

$$C(\theta, \phi) = \tfrac{1}{2}[\sin(4\phi) + \sin(2\theta) + \sin(2\theta)\cos(4\phi)]. \qquad (6)$$

θ and ϕ characterize the ellipticity of the Stokes and pump-probe fields, respectively, and are defined as the angle between the fast axis (set parallel to the x axis) of a quarter wave plate and an input linear polarization. For the experimentally practical situation where the polarization of the broadband Stokes field is constrained to be linear [i.e., $C(0, \phi)$], the difference signal $\triangle S$ is maximized for an elliptical pump polarization with $\phi = \pi/8$, $3\pi/8$. The signal-to-noise ratio can be shown to be highest for $\phi = 3\pi/8$ (see the Supplemental Material [38]), corresponding to the major axis of the ellipse being orthogonal to the Stokes polarization: this arrangement was used for the measurements shown in Figs. 2 and 3. Significantly, $\triangle S$ retains the same spectral form, regardless of the ellipticity of the excitation beams. In general, the NRB will be removed as long as the polarization ellipses are symmetric with respect to the measurement axes, while the ellipticity determines the amplitude of $\triangle S$. This decoupling of NRB removal and signal amplitude simplifies the alignment under tight focusing conditions or in the presence of sample window birefringence [6]. Polarization can be set *in situ* at the focus by iteratively minimizing the NRB and maximizing the difference signal at resonance.

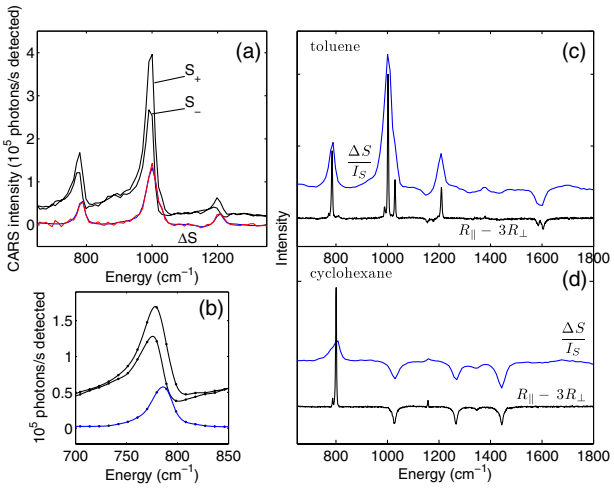

FIG. 2 (color online). (a) Interferometric correction of the NRB in toluene. S_+ and S_- are the raw CARS spectra measured along the $\hat{\mathbf{n}}_+$ and $\hat{\mathbf{n}}_-$ directions of Fig. 1(b) (10 ms exposure). The difference spectrum $\Delta S = S_+ - S_-$ contains nondispersive line shapes at the correct Raman shifts [cf. (c)] (red line, 10 ms; blue line, 100 ms). (b) Close-up of the region around 786 cm^{-1} showing the ΔS peak shifted with respect to the dispersive CARS peaks (100 ms; lines are to guide the eye). (c), (d) Comparison of normalized SIP CARS to the spontaneous Raman spectrum formed by $R_\parallel - 3R_\perp$ ($R_\parallel$, parallel polarized; $R_\perp$, perpendicular polarized). Curves are offset for clarity [(c), toluene; (d), cyclohexane]. The SIP CARS and spontaneous Raman spectra agree closely, to within the resolution of the SIP CARS measurement. Average powers are at the focus; pump, 14 mW; Stokes, 25 mW.

Experiments with an elliptical pump and broadband linear Stokes beam were performed with the apparatus detailed in Fig. 1(c), and described in detail in the Supplemental Material [38]. Both beams were derived from a Ti:sapphire oscillator (785 nm, 2 ps, 76 MHz): 10% of the output was used as the pump-probe field, while the remaining power was passed through a PCF to generate the Stokes field (800–1040 nm). A forward detection geometry was used, with illumination and collection by 1.3NA objective lenses, and with a Wollaston prism placed after the collection objective to separate the two detection polarizations on the CCD. Aberrations in the spectrometer limited the spectral resolution to 30 cm^{-1}.

Correction of Raman line shapes and removal of the NRB in SIP CARS are shown for toluene in Fig. 2(a). The two CARS spectra S_+ and S_- exhibit the asymmetric dispersive line shapes and spectrally varying NRB, which is characteristic of CARS measurements. The difference spectrum ΔS shows no NRB, and Raman peaks are symmetric and occur at the correct vibrational energy. Figure 2(b) shows this in greater detail for the mode at 786 cm^{-1} [39].

Direct comparison to spontaneous Raman spectra can be made by equating the depolarization ratio in Eq. (4) with the spontaneous Raman depolarization ratio [37,40] $\rho = R_\perp/R_\parallel$, where $R_\parallel$ and $R_\perp$ are spontaneous Raman

spectra with incident and scattered polarizations mutually parallel and perpendicular, respectively. Then, $R_{\parallel} \propto \mathrm{Im}\{\chi_{1111}\}$ and $R_{\perp} \propto \mathrm{Im}\{\chi_{1221}\}$, and from Eq. (4),

$$\frac{\Delta S}{I_S} \propto R_{\parallel} - 3R_{\perp}. \tag{7}$$

Note that the normalization of the difference spectrum by I_S corrects the peak amplitudes for variation in the Stokes spectrum to allow comparison with the spontaneous Raman spectrum; it is not necessary for removing the NRB or for quantitative measurements. For a nonresonant sample, $\chi_{1111} = \chi_{\mathrm{NR}}$ and $\chi_{1221} = \chi_{\mathrm{NR}}/3$, and Eq. (2) reduces to $P_x = \chi_{\mathrm{NR}} E_p^2 E_S^*/\sqrt{2}$ and $P_y = -i\chi_{\mathrm{NR}} E_p^2 E_S^*/3\sqrt{2}$ (where we have set $E_{pr} = E_p$). The sum spectrum ΣS is then

$$\Sigma S \propto P_x P_x^* + P_y P_y^* \propto I_p^2 I_S \chi_{\mathrm{NR}}^2. \tag{8}$$

The spectral form of I_S can therefore be determined from that of ΣS, obtained from a nonresonant medium; we have employed a glass coverslip for this purpose, as the glass resonant response is slowly varying and weakens towards higher wave numbers. We find agreement between SIP CARS and spontaneous Raman spectroscopy in terms of both spectral position and relative peak heights [shown for cyclohexane and toluene in Figs. 2(c) and 2(d)]. As expected from Eq. (5), the amplitude of each Raman line is scaled by the depolarization ratio, with peaks going negative for resonances with $\rho > 1/3$, providing a powerful approach for the differentiation of otherwise similar spectra on the basis of mode symmetry (as demonstrated for imaging in Sec. IV of the Supplemental Material [38]).

As the nonresonant response χ_{NR} amplifies the resonant CARS signal, quantitative measurements in heterogeneous media require an account to be taken of any variation of χ_{NR}, for example, as density changes across a sample. SIP CARS is self-calibrating, in that χ_{NR} can be monitored in the same measurement if a spectrum contains a nonresonant region (such as the ''quiet'' spectral region exhibited by biological samples). From Eq. (8), measuring ΣS at a reference frequency away from resonances gives a quantity $\Sigma S_{\mathrm{NR}} \propto \chi_{\mathrm{NR}}^2$. The difference spectrum can therefore be normalized by $\sqrt{\Sigma S_{\mathrm{NR}}}$ to give a signal which is linear in concentration and independent of the strength of the nonresonant response, verified experimentally from measurements of samples with strongly varying NRB (see the Supplemental Material [38]).

To demonstrate that SIP CARS is suitable for a wide range of laser systems, the method was also implemented using a commercial supercontinuum source (detailed in the Supplemental Material [38]). In this system, both pump and Stokes beams were seeded by the same low-power fiber laser oscillator and then amplified independently. One amplified output generated the Stokes beam via a long PCF, while the other was used directly as the pump field. This system served as a rigorous demonstration of the robustness of the technique, as the amplified beams contain more noise and amplified spontaneous emission than the Ti:sapphire oscillator, and the PCF generated Stokes beam has relatively low spectral coherence. Single-exposure broadband interferometric NRB removal for this system would not be possible by any other optical technique.

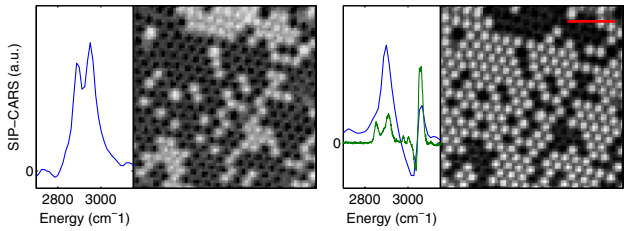

FIG. 3 (color online). Hyperspectral imaging of a sample containing both polystyrene (PS) and polymethylmethacrylate (PMMA) beads of 1 μm diameter (100 ms/pixel; 64×64 pixels; 300 nm step size. Scale bar 5 μm). Multivariate analysis was performed using Pearson clustering, and the component spectra are shown next to their corresponding intensity maps. The temporal delay between the pump and Stokes beams was chosen to maximize power in the C-H spectral region. The two bead populations can be clearly distinguished; left panel: PMMA beads; right panel: PS. Also shown for PS is the spectrum $R_{\parallel} - 3R_{\perp}$ (green). Note the SIP-CARS spectra have not been normalized by the Stokes spectrum I_S; hence, peak amplitudes differ from the spontaneous Raman measurements (larger images (126×126 pixels) taken with 10 ms exposure are shown in the Supplemental Material [38]).

Hyperspectral imaging was demonstrated on a sample containing both polystyrene (PS) and polymethylmethacrylate (PMMA) beads of 1 μm diameter. The polarized spectra S_+ and S_- were acquired simultaneously at each pixel, and the difference spectrum ΔS was then scaled by the square root of ΣS integrated over the nonresonant region 2000–2450 cm^{-1}. Pearson-based cluster analysis [41] was performed on this hyperspectral data set; the first two component spectra and their intensity maps are shown in Fig. 3. The component spectra contain all the features of the spontaneous Raman spectra of polystyrene and PMMA, and the two bead populations can be clearly distinguished.

In summary, by exploiting the third-order polarization response, SIP CARS allows acquisition of CRS spectra free of NRB, with complete agreement to spontaneous Raman measurements. Spectra are amplified by the nonresonant response and are quantitative, with a linear concentration dependence, making the technique suitable for hyperspectral imaging. The method uses only passive polarization optics, has low stability requirements, and is suitable for any laser system capable of generating CARS, permitting single-exposure interferometric NRB removal with broad PCF generated supercontinua.

This work was supported by the Biotechnology and Biological Sciences Research Council (BB/F016344) and

with funding by the European Union through the European Metrology Research Programme (NEW02-REG2). The European Metrology Research Programme (EMRP) is jointly funded by the EMRP participating countries within EURAMET and the European Union.

*bradley.littleton@kcl.ac.uk
†david.r.richards@kcl.ac.uk

[1] B. G. Saar, C. W. Freudiger, J. Reichman, C. M. Stanley, G. R. Holtom, and X. S. Xie, Science **330**, 1368 (2010).
[2] S. H. Parekh, Y. J. Lee, K. A. Aamer, and M. T. Cicerone, Biophys. J. **99**, 2695 (2010).
[3] X. J. Cheng and X. S. Xie, J. Phys. Chem. B **108**, 827 (2004).
[4] G. L. Eesley, *Coherent Raman Spectroscopy* (Pergamon, New York, 1981), Vol. 9.
[5] E. Nordstrom, A. Bohlin, and P.-E. Bengtsson, J. Raman Spectrosc., doi:10.1002/jrs.4275.
[6] S. Roy, J. R. Gord, and A. K. Patnaik, Prog. Energy Combust. Sci. **36**, 280 (2010).
[7] C. W. Freudiger, W. Min, B. G. Saar, S. Lu, G. R. Holtom, C. He, J. C. Tsai, J. X. Kang, and X. S. Xie, Science **322**, 1857 (2008).
[8] M. N. Slipchenko, R. A. Oglesbee, D. Zhang, W. Wu, and J.-X. Cheng, J. Biophotonics **5**, 801 (2012).
[9] H. Kano and H. Hamaguchi, Appl. Phys. Lett. **86**, 121113 (2005).
[10] J. P. R. Day, K. F. Domke, G. Rago, H. Kano, H.-o. Hamaguchi, E. M. Vartiainen, and M. Bonn, J. Phys. Chem. B **115**, 7713 (2011).
[11] S. A. Akhmanov, A. F. Bunkin, S. G. Ivanov, and N. I. Koroteev, JETP Lett. **25**, 416 (1977).
[12] J.-L. Oudar, R. W. Smith, and Y. R. Shen, Appl. Phys. Lett. **34**, 758 (1979).
[13] F. Vestin, M. Afzelius and P.-E. Bengtsson, Proc. Combust. Inst. **31**, 833 (2007).
[14] F. Lu, W. Zheng, and Z. Huang, Opt. Lett. **33**, 2842 (2008).
[15] A. Volkmer, L. D. Book, and X. S. Xie, Appl. Phys. Lett. **80**, 1505 (2002).
[16] S. Roy, T. R. Meyer, and J. R. Gord, Appl. Phys. Lett. **87**, 264103 (2005).
[17] Y. J. Lee and M. T. Cicerone, Appl. Phys. Lett. **92**, 041108 (2008).
[18] M. Cui, B. R. Bachler, and J. P. Ogilvie, Opt. Lett. **34**, 773 (2009).
[19] E. O. Potma, C. L. Evans, and X. S. Xie, Opt. Lett. **31**, 241 (2006).
[20] C. Muller, T. Buckup, B. von Vacano, and M. Motzkus, J. Raman Spectrosc. **40**, 809 (2009).
[21] M. Jurna, J. P. Korterik, C. Otto, J. L. Herek, and H. L. Offerhaus, Opt. Express **16**, 15863 (2008).
[22] K. Orsel, E. T. Garbacik, M. Jurna, J. P. Korterik, C. Otto, J. L. Herek, and H. L. Offerhaus, J. Raman Spectrosc. **41**, 1678 (2010).
[23] T. W. Kee, H. Zhao, and M. T. Cicerone, Opt. Express **14**, 3631 (2006).
[24] S.-H. Lim, A. G. Caster, and S. R. Leone, Phys. Rev. A **72**, 041803 (2005).
[25] D. Oron, N. Dudovich, and Y. Silberberg, Phys. Rev. Lett. **90**, 213902 (2003).
[26] C. L. Evans, E. O. Potma, and X. S. N. Xie, Opt. Lett. **29**, 2923 (2004).
[27] P. D. Chowdary, W. A. Benalcazar, Z. Jiang, D. M. Marks, S. A. Boppart, and M. Gruebele, Anal. Chem. **82**, 3812 (2010).
[28] J. Sung, B.-C. Chen, and S.-H. Lim, J. Raman Spectrosc. **42**, 130 (2011).
[29] D. Oron, N. Dudovich, and Y. Silberberg, Phys. Rev. Lett. **89**, 273001 (2002).
[30] A. Wipfler, J. Rehbinder, T. Buckup, and M. Motzkus, Opt. Lett. **37**, 4239 (2012).
[31] E. M. Vartiainen, H. A. Rinia, M. Muller, and M. Bonn, Opt. Express **14**, 3622 (2006).
[32] Y. Liu, Y. J. Lee, and M. T. Cicerone, Opt. Lett. **34**, 1363 (2009).
[33] M. T. Cicerone, K. A. Aamer, Y. J. Lee, and E. Vartiainen, J. Raman Spectrosc. **43**, 637 (2012).
[34] L. Lepetit, G. Chériaux, and M. Joffre, J. Opt. Soc. Am. B **12**, 2467 (1995).
[35] W. Langbein, I. Rocha-Mendoza, and P. Borri, Appl. Phys. Lett. **95**, 081109 (2009).
[36] D. A. Kleinman, Phys. Rev. **126**, 1977 (1962).
[37] D. Gachet, N. Sandeau, and H. Rigneault, J. Eur. Opt. Soc. **1**, 06013 (2006).
[38] See Supplemental Material at http://link.aps.org/supplemental/10.1103/PhysRevLett.111.103902 for derivation of the SIP CARS amplitude for arbitrary ellipticities, signal-to-noise ratio analysis, experimental details, concentration dependence, and further imaging results.
[39] J. K. Wilmshurst and H. J. Bernstein, Can. J. Chem. **35**, 911 (1957).
[40] M. A. Yuratich and D. C. Hanna, Mol. Phys. **33**, 671 (1977).
[41] A. Almahdy, F. Downey, S. Sauro, R. Cook, M. Sherriff, D. Richards, T. Watson, A. Banerjee, and F. Festy, Caries Research **46**, 432 (2012).